Physics   College of Arts and Sciences

Interacting Topological Defects on Frozen Topographies

Mark Bowick
Department of Physics, Syracuse University, Syracuse, NY

David R. Nelson
Harvard University

Alex Travesset
Syracuse University

Interacting Topological Defects on Frozen Topographies

Mark J. Bowick[(1,2)*] David R. Nelson[(2)†]and Alex Travesset[(1)‡]
[1]Physics Department, Syracuse University,
Syracuse, NY 13244-1130, USA
[2]Lyman Laboratory of Physics, Harvard University,
Cambridge, MA 02138, USA

Abstract

We propose and analyze an effective free energy describing the physics of disclination defects in particle arrays constrained to move on an arbitrary two-dimensional surface. At finite temperature the physics of interacting disclinations is mapped to a Laplacian Sine-Gordon Hamiltonian suitable for numerical simulations. We then specialize to the case of a spherical crystal at zero temperature. The ground state is analyzed as a function of the ratio of the defect core energy to the Young's modulus. We argue that the core energy contribution becomes less and less important in the limit $R \gg a$, where R is the radius of the sphere and a is the particle spacing. For large core energies there are twelve disclinations forming an icosahedron. For intermediate core energies unusual finite-length grain boundaries are preferred. The complicated regime of small core energies, appropriate to the limit $R/a \to \infty$, is also addressed. Finally we discuss the application of our results to the classic Thomson problem of finding the ground state of electrons distributed on a two-sphere.

[*]bowick@physics.syr.edu
[†]nelson@cmt.harvard.edu
[‡]alex@suhep.phy.syr.edu

1

1 Introduction

The theory of two-dimensional melting of essentially planar materials (monolayers) is a rich and well-developed subject [1, 2]. An interesting aspect of melting in this low dimension is that both the crystalline to hexatic and hexatic to fluid transitions can be driven by the sequential liberation of point-like topological defects – dislocations in the former case and disclinations in the latter. It is clearly important, therefore, to have a thorough understanding of the statistical mechanics of interacting topological defects. On the plane all topological defects are bound at zero temperature, but on manifolds with more complicated topology excess free disclinations must exist even at zero temperature.

The statistical mechanics of particles confined to frozen surfaces of constant positive and negative curvature was discussed, e.g. in references [3] and [4]. It was argued that regions of positive and negative curvature would promote the formation of unpaired disclinations, and that these might be screened by clouds of dislocations. At low temperature, it was suggested that the anisotropic interaction between these screening dislocations would lead them to condense into grain boundaries. The physics of particles on a quenched *random* topography was discussed in Ref.[5].

The simplest example of a surface with positive Gaussian curvature is the sphere. Dodgson studied the ground state of the Abrikosov flux lattice in a model thin film superconductor on a sphere (subject to a field radiating from a magnetic monopole at the center), and found evidence for twelve five-fold disclination defects at the vertices of an icosahedron in an otherwise six-coordinated crystalline environment [6]. This defect configuration is similar to one proposed by Lubensky and collaborators for lipid bilayer vesicles in the hexatic phase [7], except that in hexatics the disclination energy is reduced by screening due to an equilibrium concentration of unbound dislocations. Later, Dodgson and Moore proposed adding dislocations to the ground state of a sufficiently large vortex crystal in a spherical geometry to screen out the strains associated with twelve extra disclinations in the Abrikosov phase [8]. Vortices in a thin film superconductor behave like particles interacting with a repulsive logarithmic pair potential. Another context in which crystalline ground states on a sphere arise is the so-called *Thomson problem*, where the vortices are replaced by particles interacting with a repulsive $1/r$ potential [9, 10, 11]. Our own interest in this class of problems was stimulated by the beautiful work of Alar Toomre [12], which we discuss later (and which

hopefully will be described by Toomre himself one day!). Toomre's ideas also play a key role in a recent paper on the Thomson problem by Pérez-Garrido and Moore [13]. For a discussion of disclination and dislocation defects for disk-like configurations of electrons in the plane see [14].

The study of melting and the nature of the ground state on curved manifolds may be a good testing ground for understanding the new features that arise from the topological defects required for particle arrays on surfaces with nontrivial topologies. Our approach is to work directly with the defects themselves, and treat the particles within continuum elastic theory. This approach is more general than, say, a direct simulation of particles interacting with a logarithmic or $1/r$ potential, because all details of the pair potential are embodied in the elastic constants mediating the interaction between defects. By eliminating explicit reference to the particles themselves, we also greatly reduce the number of degrees of freedom needed to study the ground state. As we shall see, the effective Hamiltonian used here, in which defects such as grain boundaries and dislocations are built up out of elementary disclinations, leads to a variety of interesting and novel structures not encountered in the plane.

The statistical mechanics of monolayers on curved surfaces such as the sphere may also be viewed as the infinite bending rigidity limit of membranes with a spherical topology. Our investigation may therefore be considered a prelude to the careful incorporation of defects in the study of the phase transitions of, e.g., membranes composed of lipid bilayers [15].

It is useful to review expectations for low temperature configurations of crystals in flat space [16]. Although the ground state is believed to be defect free, one can certainly consider the response to adding a single excess disclination. The stresses induced by such a disclination are very high, and the energy can be lowered by polarizing the surrounding medium into dislocation pairs, as indicated schematically in Fig. 1.

When interactions between dislocations are taken into account one might expect them to organize into grain boundaries (i.e., lines of dislocations with Burgers vectors oriented perpendicular to the lines) to minimize the energy even further. Experiments on smectic liquid crystal films with tilted molecules [17] (the tilt is used to force in an extra disclination) reveal a pattern of five jagged grain boundaries radiating outward, consistent with this picture. Computer simulations with periodic boundary conditions have been used to study the relaxation of a disclination quartet (two fives and two sevens), from an initial configuration where these defects sit on the corners of a
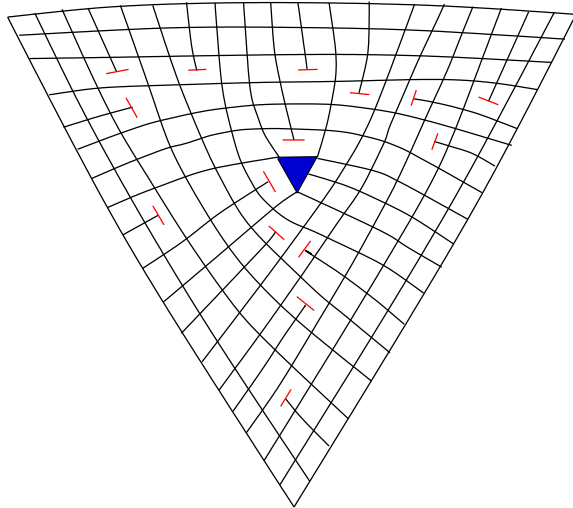
Figure 1: Schematic of an isolated threefold disclination, in an approximately four-coordinated medium. The elastic stress in the vicinity of the isolated disclination is relieved by the formation of a screening cloud of dislocations.

very large square in an otherwise six-coordinated medium [18]. After the relaxation, grain boundaries joining the fives to the sevens appear. Relaxation of the disclination elastic stresses in this way occurs at a price – the core energies associated with the extra dislocations lead to an additional term in the energy which diverges linearly with system size R, as compared to the R^2 divergence associated with an unscreened disclination [19].

A situation reminiscent of these flat space experiments occurs on surfaces of non-zero Gaussian curvature, e.g., the sphere. Although the Gaussian curvature of the sphere approximately compensates the strains associated with isolated disclinations, for small core energies (or, equivalently, large sphere radius compared to the particle spacing) it can still be favorable to introduce extra screening dislocations into the ground state.

To see how screening of an isolated five-fold disclination by dislocations comes out on a sphere, it is helpful to first consider what happens in flat space. A five-fold disclination can be created by removing a wedge of material subtending an angle $s = 2\pi/6$ and then deforming the remaining material to close the gap. (The disclination in the square lattice of Fig.1 was made by removing a $2\pi/4 = 90°$ wedge). The resulting stresses were calculated, e.g., in Ref. [20]. We use polar coordinates r and ϕ, measured from the center

4

of the disclination. If μ and λ are the material elastic constants, the stress tensor is dominated by $\sigma_{\phi\phi}$, where (neglecting logarithmic corrections due to boundary effects),

$$\sigma_{\phi\phi} = \frac{K_0 s}{4\pi} \,, \tag{1}$$

and K_0, the Young's modulus, is related to the Lamé coefficients by

$$K_0 = \frac{4\mu(\mu + \lambda)}{2\mu + \lambda} \,. \tag{2}$$

Note that $\sigma_{\phi\phi}$ is proportional to the disclination charge s. This approximately constant stress arises from the stretching of material required to close the gap engendered by the missing wedge, and leads to the R^2 divergence in disclination energy with system size R [20]. Consider now the fate of a tightly bound dislocation pair (the Burgers' vectors are equal and opposite with $|\vec{b}| = a$) placed in the stress field of this disclination. The stress $\sigma_{\phi\phi}$ creates a Peach-Kohler force which tries to tear the dislocation pair apart [21]. We assume for simplicity a purely radial separation Δr between dislocations with Burgers' vectors in the tangential direction. The energy of the pair then consists of $2E_d$ (E_d is the dislocation core energy), a logarithmic binding energy and a linear Peach-Kohler term (proportional to $\sigma_{\phi\phi}$) which tries to "ionize" the pair, similar to the effect of an electric field on a charge dipole,

$$E_{pair}(\Delta r) = 2E_d + \frac{K_0 b^2}{4\pi}\ln(\frac{\Delta r}{a}) - \frac{K_0 b}{4\pi}s(\Delta r) \,. \tag{3}$$

The energy can be lowered once Δr exceeds $\Delta r^* \approx b/s \approx a$ and the pair separates [22]. One of the liberated dislocations moves off to infinity while the other remains to help screen the disclination. As more and more dislocations are created in this way, the stress is reduced until the dislocation density n_d in an annulus of width dr at radius r from the disclination is [21]

$$n_d(r) \approx (\frac{s}{2\pi})\frac{1}{ra} \,. \tag{4}$$

Note that if these dislocations collapse to form a single linear grain boundary radiating out from the disclination, the angular deficit s is related to the spacing l between dislocations in the grain by $s \approx a/l$. If the dislocations form m grain boundaries, the spacing will be $l \approx am/s$. In this paper we shall study the cases $m = 2$ and $m = 5$.

The analysis sketched above is easily adapted to the curved surface of a sphere of radius R. The angular deficit s associated with a circuit around a dislocation in flat space can now be compensated by the nonzero Gaussian curvature $1/R^2$. Let us assume that a five-fold disclination is placed at the north pole of the sphere. We describe the physics by geodesic polar coordinates (r, ϕ) about this point with metric

$$ds^2 = dr^2 + R^2\sin^2(\frac{r}{R})d\phi^2 \,, \tag{5}$$

and work in the limit $R \gg a$. We expect that the stress is controlled by the *effective* disclination charge inside a circuit at fixed geodesic distance r from the disclination (see Eq.(13) below), namely

$$
\begin{aligned}
s_{eff}(r) &= s - \int_0^{2\pi} \mathrm{d}\phi \int_0^r \mathrm{d}r' \sqrt{g}\, K \\
&= s - \frac{2\pi}{R^2} \int_0^r R\sin(\frac{r'}{R})\mathrm{d}r' = \frac{\pi}{3} - 4\pi\sin^2(\frac{r}{2R}) \,.
\end{aligned}
\tag{6}
$$

Note that $s_{eff}(r)$ decreases with increasing r. In the limit of weak curvature $R \gg a$, we expect that the stress formula (1) is replaced by

$$\sigma_{\phi\phi}(r) = K_0 \frac{s_{eff}(r)}{4\pi} \,, \tag{7}$$

with a corresponding weakening of the Peach-Kohler force. The reduction in the angular stress $\sigma_{\phi\phi}$ with increasing geodesic distance from the disclination arises because the stretching required to remove a wedge in flat space is reduced according to the metric (5). We now expect the dislocations in m grain boundaries radiating from a disclination to exhibit a *variable* spacing between dislocations,

$$l(r) \approx \frac{am}{s_{eff}(r)} \,. \tag{8}$$

Note that the spacing diverges as $r \to r_c^-$, where

$$\frac{r_c}{R} \equiv \Theta_c = \cos^{-1}\frac{5}{6} = 33.56° \,. \tag{9}$$

The angular jump $\Delta s(r) = s_{eff}/m$ across the grain boundaries thus becomes smaller with increasing r and these boundaries eventually terminate when

6

the dislocations become sufficiently dilute. The total number of dislocations contained in the m grain boundaries is approximately

$$N_d \sim \frac{R}{a} s(\mathbf{x}) \, . \tag{10}$$

Our calculations support this picture, and we find that the extra dislocations seem to form grain boundaries. Remarkably, and in contrast to flat space, these grain boundaries do indeed stop or start inside the crystalline medium. Our results also hint at a branching pattern of grain boundary networks (each radiating from a disclination), reminiscent of those found in Ref. [17].

The paper is organized as follows. In section 2 we develop a formalism whose basic degrees of freedom are the defects themselves, rather than the underlying interacting particles. The particles themselves are treated within continuum elastic theory. As mentioned above, such a formalism has the advantage of reducing the number of degrees of freedom as well as being rather universal in the sense that it applies to a broad class of interaction potentials. Varying the pair potential simply corresponds to changing the elastic moduli and defect core energy of the model. The model has the advantage that defects can move directly to positions which minimize the energy, without the constraints associated with disclination motion or dislocation climb in a crystalline medium which would attend a particle simulation. Despite its simplicity, finite temperature statistical mechanics of this model is still not amenable to a direct analytic solution. A duality mapping to an equivalent Laplacian Sine-Gordon model, however, yields a model with short range interactions whose lattice version should be straightforward to simulate numerically.

In contrast, the limit of zero temperature may be treated analytically and we turn to this in the next three sections of the paper. In particular we discuss the ground state of a spherical crystal as a function of defect core energy relative to the combination of elastic constants (Young's modulus) which determines defect interactions at large distances.

In section 6 we shift our attention from defects alone to the underlying lattice structure. We first discuss lattices with icosahedral symmetry. Our formalism applied to this case predicts the range of core energies for which the lattice is unstable to the formation of defects.

An interesting application for our formalism is to the *Thomson* problem [9, 10], discussed in section 7. The predictions of our approach are in agreement with existing results where comparisons are available. A beautiful ex-

7

perimental realization of the Thomson problem is provided by multi-electron bubbles trapped in liquid helium at low temperatures [23]. Order in electrons confined by a positively charged capacitor plate to a helium surface has been studied for many years. Except for capillary wave deformations, crystallization proceeds in an essentially flat environment. At high electron densities, curvature is introduced via an instability to a regular array of "dimples" in the helium surface, each containing a million electrons or more. Upon increasing the density of positive charge below the surface further by adding a metallic tip to the anode, one can form completely submerged multi-electron spherical bubbles. Typical bubbles contain 10^6-10^8 electrons. The outward electrostatic repulsion of the electrons on the inner surface of the helium bubble balances against the surface tension of the helium interface to produce bubbles with diameters in the range $10-100$ microns. Results for the Thomson problem have implications for trapped multi-electron bubbles well below the flat space freezing temperature.

2 Finite Temperature

2.1 Free Energy

As our main interest lies in the study of defects on two-dimensional curved surfaces, we need a formalism that deals directly with the defect degrees of freedom themselves. A rigorous geometrical derivation of the effective free energy for the defects is given in [24]. An equivalent derivation may also be given by integrating out the phonon degrees of freedom from the elastic Hamiltonian [25], with the appropriate modifications for a general distribution of defects. The energy of a two-dimensional crystal embedded in an arbitrary frozen geometry described by a metric $g_{ij}(\mathbf{x})$ is given by

$$
\begin{aligned}
E &= K_0 \int d^2\mathbf{x}\sqrt{g(\mathbf{x})}d^2\mathbf{y}\sqrt{g(\mathbf{y})}(K(\mathbf{x}) - s(\mathbf{x})) \left.\frac{1}{\Delta^2}\right|_{\mathbf{xy}} (K(\mathbf{y}) - s(\mathbf{y})) \\
&+ K_A \int d^2\mathbf{x}\sqrt{g(\mathbf{x})}d^2\mathbf{y}\sqrt{g(\mathbf{y})}(K(\mathbf{x}) - s(\mathbf{x})) \left.\frac{1}{\Delta}\right|_{\mathbf{xy}} (K(\mathbf{y}) - s(\mathbf{y})) (11)
\end{aligned}
$$

where $g(\mathbf{x})$ is the determinant of the metric tensor, $K(\mathbf{x})$ is the associated Gaussian curvature and $s(\mathbf{x})$ the disclination density

$$
s(\mathbf{x}) = \frac{\pi}{3\sqrt{g(\mathbf{x})}} \sum_{i=1}^{N} q_i \delta(\mathbf{x}, \mathbf{x}_i) \ , \tag{12}
$$

with N disclinations located at the sites $\mathbf{x}_i$ of an underlying triangulated particle array. The "charges" q_i may be positive or negative. Although we do not restrict the allowed values of the charge, we expect the unit charge defects to dominate for energetic reasons. A plus one charge corresponds to a five-fold coordinated particle (a five-disclination) and a minus one charge corresponds to a seven-fold coordinated particle (a seven-disclination). Charges are attracted to regions of *like-sign* Gaussian curvature.

The first term of Eq. (11) represents a long range elastic interaction and K_0 is the Young's modulus of Eq. (2) [25].

The second term in Eq. (11) contains a single inverse-Laplacian operator, which is singular at short distances due to distortions of the lattice at distances less than the lattice spacing. This is the dominant term for hexatic membranes, where K_A is the hexatic stiffness.[25] In the present context, this singular contribution leads to a renormalized core energy $E_{core}(K_A)$ for each defect and it represents non-universal details of the interaction on the scale of the inter-particle spacing a. The energy of Eq. (11) is thus simplified to

$$
\begin{aligned}
E(K_0) &= K_0 \int d^2\mathbf{x}\sqrt{g(\mathbf{x})}d^2\mathbf{y}\sqrt{g(\mathbf{y})}(K(\mathbf{x}) - s(\mathbf{x}))\left.\frac{1}{\Delta^2}\right|_{\mathbf{xy}}(K(\mathbf{y}) - s(\mathbf{y})) \\
&+ N\,E_{core}\ .
\end{aligned}
\tag{13}
$$

Although it is not essential, we assume for convenience that the core energies of five and seven-fold disclinations are identical. The partition function of our model is then

$$
\mathcal{Z}(\beta) = \sum_{N_+,N_-}\frac{\delta_{N_+-N_-,6\chi}}{N_+!N_-!}y^{N_++N_-}\int\prod_{\mu=1}^{N_+}d\mathbf{x}_\mu^+\sqrt{g}\prod_{\nu=1}^{N_-}d\mathbf{x}_\nu^-\sqrt{g}e^{-\beta E(K_0)}\ ,
\tag{14}
$$

where $E(K_0)$ is the first term in Eq. (13), y is the disclination fugacity $e^{-\beta E_{\text{core}}}$ (β is the inverse temperature), $N_\pm$ is the total number of fives and sevens respectively and χ is the Euler characteristic of the surface. For a given microscopic interaction potential both y and K_0 are fixed. We shall find it useful, however, to regard these as independent parameters and discuss, in particular, the limits of large and small E_{core} compared to K_0a^2, where a is the lattice constant.

Despite its elegant form this model is difficult to solve analytically. It is, moreover, challenging for direct numerical simulation because of the long-range interaction embodied in $1/\Delta^2$ – see the explicit form for $E(K_0)$ given in Eqs. (28) and (29) below. An alternative formulation is suggested by the

9

Laplacian roughening model for flat space melting [26, 27]. Direct molecular dynamics simulations or energy evaluations of particles interacting with a specified potential [28, 12] are also of considerable interest. Since this approach takes the particles as the primary degrees of freedom, rather than the defects, it falls outside the scope of the present paper.

2.2 The Sine-Gordon model

We now restrict ourselves to the case of the sphere, which has Euler characteristic $\chi = 2$. We map the previous model to a dual Sine-Gordon model with only short range interactions by adapting the derivation presented in [29] to the present case, with some additional improvements.

Let us start with the identity

$$
\begin{aligned}
& e^{-\frac{\beta}{2}\int \sqrt{g}du\sqrt{g}dv(s(u)-K(u))\frac{1}{\Delta^2}(s(v)-K(v))} \\
= \; & (det'\Delta^2)\int \mathcal{D}\phi' e^{-\frac{1}{2\beta}\int du\sqrt{g}\Delta\phi\Delta\phi}e^{-i\int du\sqrt{g}\phi(u)(s(u)-K(u))}
\end{aligned}
\tag{15}
$$

The topological constraints ensure that the zero mode does not contribute to the path integral and this is indicated by the primes in the determinant and the measure.

Since the zero mode is the constant eigenvector of the Laplacian, orthonormality implies that

$$
\int du\sqrt{g}\phi = 0
\tag{16}
$$

for any configuration ϕ included in the measure of the path integral in Eq. (15).

With this identity Eq. (14) becomes

$$
\mathcal{Z}(\beta) = \int \mathcal{D}\phi' \mathcal{F}(\phi)e^{-\frac{1}{2\beta}\int du\sqrt{g}\Delta\phi\Delta\phi}e^{-i\int du\sqrt{g}\phi K(u)} \equiv \int \mathcal{D}\phi' e^{-\mathcal{H}(\phi)} \; ,
\tag{17}
$$

where the last identification defines the Hamiltonian $\mathcal{H}(\phi)$ and $\mathcal{F}(\phi)$ is given by

$$
\begin{aligned}
\mathcal{F} &= \sum_{N_+,N_-} \frac{\delta_{N_+-N_-,12}}{N_+!N_-!} y^{N_++N_-} \int \prod_{\mu=1}^{N_+} d\mathbf{x}_\mu^+ \sqrt{g} \prod_{\nu=1}^{N_-} d\mathbf{x}_\nu^- \sqrt{g} e^{\frac{i\pi}{3}(\phi(\mathbf{x}_\mu^+)-\phi(\mathbf{x}_\nu^-))} \\
&= \sum_{N_+,N_-} \frac{\delta_{N_+-N_-,12}}{N_+ N_-} (y\int du\sqrt{g}e^{\frac{i\pi}{3}i\phi(u)})^{N_+}(y\int du\sqrt{g}e^{\frac{-i\pi}{3}i\phi(u)})^{N_-}
\end{aligned}
\tag{18}
$$

10

Upon writing the Kronecker delta as

$$\delta_{N_+-N_-,12} = \int_0^1 dx \ e^{-i2\pi x(N_+-N_--12)} \ , \tag{19}$$

one finds

$$\mathcal{F}(\phi) = \int_0^1 dx \ e^{-i12x} e^{\int du\sqrt{g}\cos(\frac{\pi}{3}\phi(u)+x)} \tag{20}$$

Inserting this result in Eq. (17) and performing the integral over the x variable leads to

$$\mathcal{H}(\phi) = \frac{1}{2\beta}(\frac{3}{\pi})^2 \int du\sqrt{g}\Delta\phi\Delta\phi - 2y \int du\sqrt{g}\cos\phi + \frac{3i}{\pi} \int du\sqrt{g}K\phi \ . \tag{21}$$

The last (imaginary) term is a nuisance for practical applications. For the case of the sphere, however, the Gaussian curvature is constant, and we have

$$\int du\sqrt{g}K\phi = K \int du\sqrt{g}\phi = 0 \ , \tag{22}$$

where we have used Eq. (16). The Sine-Gordon representation for the sphere takes a very simple form

$$\mathcal{H}(\phi) = \frac{1}{2\beta}(\frac{3}{\pi})^2 \int du\sqrt{g}\Delta\phi\Delta\phi - 2y \int du\sqrt{g}\cos\phi \ . \tag{23}$$

Discretizing this expression for large y will yield a simple model with integer variables $\phi(u)$. A numerical simulation of this model seems the appropriate way to study the finite temperature statistical mechanics of defect arrays on a sphere [26, 27].

We now turn to the limiting case of zero temperature.

3 Zero Temperature Limit

3.1 General Surfaces

The zero temperature limit requires the determination of the ground state by a minimization of the energy as a function of both the position and total number of defects.

For the minimization with respect to the location of defects we see that the energy Eq. (13) depends only on the difference between the geometric

curvature and the defect density. As a result the defects will arrange themselves to approximately match the Gaussian curvature determined by the geometry of the confining surface. A complete screening of the Gaussian curvature would yield a crystal with zero elastic energy at zero temperature. An important example is that of a crystal with the symmetry of a perfect icosahedron. The twelve positive disclinations located at its twelve vertices compensate the Gaussian curvature. There are twelve five-fold coordinated particles at the vertices, and all the rest are six-fold coordinated.

As for the minimization with respect to total defect number, it is clear that the second term of Eq. (13) is linear with the number of defects, and so will clearly favor the lowest possible number of them. The physics of the zero temperature limit is therefore controlled by the competition between the core energy cost of creating a defect and the compensating gain from the screening of Gaussian curvature when defects are allowed to proliferate.

3.2   The spherical crystal

From now on we concentrate on a spherical crystal. Since the sphere has Euler characteristic 2 (genus 0) the charges q_i of a set of disclinations must satisfy

$$\int d^2\mathbf{x}\sqrt{g(\mathbf{x})}s(\mathbf{x}) = 4\pi \rightarrow \sum_{i=1}^{N} q_i = 12 \ . \tag{24}$$

This implies that, even at zero temperature, a sphere contains at least twelve excess five-fold disclinations.

To evaluate the free energy Eq. (11) we compute first the inverse square-Laplacian operator on a sphere of radius R,

$$\frac{1}{4\pi}\chi(\theta^a, \phi^a; \theta^b, \phi^b) = \frac{1}{\Delta^2} = R^2 \sum_{l=1}^{\infty} \sum_{m=-l}^{l} \frac{Y_m^l(\theta^a, \phi^a)Y_m^{l*}(\theta^b, \phi^b)}{l^2(l+1)^2} \ , \tag{25}$$

where $Y_m^l(\theta, \phi)$ are the spherical harmonics and (θ, ϕ) are the usual spherical angles. The $l = 0$ term does not appear in the sum, again as a result of the precise topology of the sphere (Eq. (24)). The absence of this zero mode leads to a finite sum. The expression Eq. (25) may also be written

$$\chi(\theta^a, \phi^a; \theta^b, \phi^b) \equiv \chi(\beta) = R^2 \sum_{l=1}^{\infty} \frac{2l+1}{l^2(l+1)^2} P_l(\cos\beta) \ , \tag{26}$$

where

$$\cos\beta = \cos\theta^a \cos\theta^b + \sin\theta^a \sin\theta^b \cos(\phi^a - \phi^b) \tag{27}$$

gives the length β of the geodesic arc connecting (θ^a, ϕ^a) and (θ^b, ϕ^b) on the sphere. It is shown in Appendix B that this last sum may be written [30]

$$\chi(\theta^a, \phi^a; \theta^b, \phi^b) = R^2 \left(1 + \int_0^{\frac{1-cos\beta}{2}} dz \, \frac{\ln z}{1-z} \right) . \tag{28}$$

In Appendix A we discuss the flat space limit of infinite sphere radius. In Fig. 2 we plot χ/R^2 (Eq. (28)) as a function of the geodesic distance β. Although the formula Eq. (28) is simple, it is not particularly suitable for rapid numerical evaluation. In Appendix C we give alternative expressions for χ better suited to fast numerical evaluation.

The final expression for the total energy of a spherical crystal with an arbitrary number of disclinations follows from Eq. (28) and Eq. (13):

$$E(K_0) = \frac{\pi K_0}{36} R^2 \sum_{i=1}^{N} \sum_{j=1}^{N} q_i q_j \chi(\theta^i, \phi^i; \theta^j, \phi^j) + N \, E_{core} . \tag{29}$$
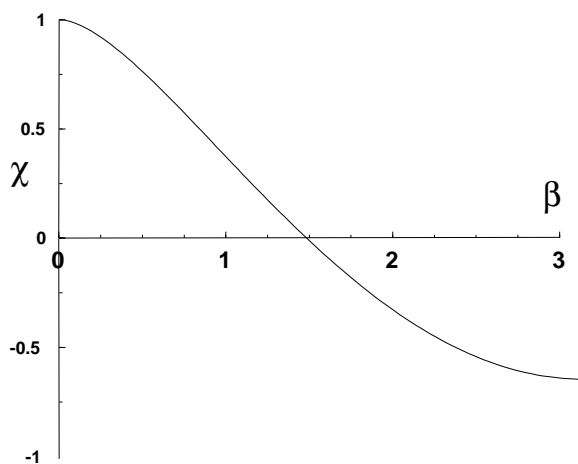

Figure 2: Plot of χ/R^2 as a function of the geodesic angle β. Only the interval $\beta \in [0, \pi]$ is plotted.

Our interpretation of the disclination density screening out the Gaussian curvature can be made more precise. Note that

$$s(\mathbf{x}) \;\; = \;\; \frac{\pi}{3\sqrt{g}} \sum_{i=1}^{N} q_i \delta(\mathbf{x}, \mathbf{x}_i)$$

13

$$
= \frac{1}{R^2} + \frac{\pi}{3R^2} \sum_{l=1}^{\infty} \sum_{m=-l}^{l} Y_m^l(\theta, \phi) \sum_{i=1}^{N} q_i Y_m^{l*}(\theta_i, \phi_i) \tag{30}
$$

$$
= K(\mathbf{x}) + \frac{\pi}{3R^2} \sum_{l=1}^{\infty} \sum_{m=-l}^{l} Y_m^l(\theta, \phi) \sum_{i=1}^{N} q_i Y_m^{l*}(\theta_i, \phi_i),
$$

where the topological constraint Eq. (24) has been used. This last identity makes it clear that the set of equations

$$
\sum_{i=1}^{N} q_i Y_m^l(\theta_i, \phi_i) = 0 , \tag{31}
$$

for all $l \geq 1$ and all m, is the condition that the disclination density exactly matches the Gaussian curvature. Because it is difficult to imagine how discrete disclination charges could exactly cancel a smooth background Gaussian curvature, we cannot expect that Eq.(31) will be satisfied in general for all values of l. We will, however, give examples where this set of equations is partially satisfied. It is easy to see, in fact, that in the limit of vanishing core energies, a configuration of defects satisfying Eq. (31) is an absolute minimum of the energy Eq. (29), since the latter can be rewritten as

$$
E = \frac{\pi^2 K_0}{9} R^2 \sum_{l=1}^{\infty} \sum_{m=-l}^{l} \frac{\left| \sum_{i=1}^{N} q_i Y_m^l(\theta_i, \phi_i) \right|^2}{l^2(l+1)^2} + N\, E_{core} . \tag{32}
$$

Eq. (31) then implies, for $E_{core} = 0$, that the energy attains its minimum value of 0.

Finally, we note that an equivalent expression for Eq. (29) is given by

$$
E = \frac{\pi K_0}{36} R^2 \sum_{l=1}^{\infty} \frac{2l+1}{l^2(l+1)^2} \sum_{i=1}^{N} \sum_{j=1}^{N} q_i q_j P_l(\cos \beta_{ij}) + N\, E_{core} . \tag{33}
$$

Eqs. (32) and (29) are useful because they express the total energy as a sum of individual l-mode contributions

$$
E = \sum_{l=1}^{\infty} E_l , \tag{34}
$$

with the order of magnitude of each l-mode coefficient being roughly

$$
E_l \sim \frac{2l+1}{l^2(l+1)^2} . \tag{35}
$$

14

By considering increasingly exotic arrangements of defects, we might hope to satisfy Eq. (31) for more and more low l-modes. If we do not enhance the large-l contributions and do not pay too large a price in defect core energy, then the total energy will be small.

4 Large core energies: The icosahedral lattice

In the limit of large core energies the creation of additional defects will be strongly penalized and the sphere will contain only the minimum allowed twelve positive disclinations. From symmetry considerations it is a good ansatz to assume that these twelve disclinations minimize the repulsive χ potential acting between them by forming an icosahedron $\mathcal{I}$ [6, 7]. It is not difficult to check that the icosahedron is in fact an extremum of the energy Eq. (29)

$$\left.\frac{\partial E}{\partial \theta_i}\right|_{\mathcal{I}} = 0 \quad , \quad \left.\frac{\partial E}{\partial \phi_i}\right|_{\mathcal{I}} = 0 \ , \tag{36}$$

where $i = 1, \cdots, 12$. We have checked numerically that fluctuations around this extremum increase the energy. Allowing the fluctuations to relax results in fast convergence to the icosahedron. Our numerical minimization gives the icosahedron as a global minimum. Thus our model successfully predicts an icosahedron minimum in the case where just twelve disclinations are allowed.

From Eq. (32) the energy is a function of the quantity

$$V_m^l(\mathcal{I}) = \sum_{i=1}^{12} Y_m^l(\theta_i, \phi_i) \ , \quad m = -l, \cdots, l \tag{37}$$

where $(\theta_i, \phi_i)_{i=1,\cdots,12}$ are particular coordinates for an icosahedron $\mathcal{I}$ on the sphere. This solution is obviously invariant under the full icosahedral group plus inversions, $\mathcal{Y}_h = \mathcal{Y} \times C_i$. Since $\mathcal{Y}$ is contained in $SO(3)$, we can construct a representation of $\mathcal{Y}$ out of the irreducible representations of $SO(3)$. We have

$$\sum_{m'=-l}^{l} D_{mm'}^l(g_Y) V_{m'}^l = 1 \cdot V_m^l \ , \tag{38}$$

where g_Y is any element belonging to $\mathcal{Y}$. That is, V_m^l is a singlet of the icosahedral group $\mathcal{Y}$. This in turn means that if the trivial representation

(the so-called A representation) of the icosahedral group is not contained as an induced representation from the full rotational group, then Eq.(31) is exactly satisfied for any twelve disclinations forming an icosahedron,

$$V_m^l = \sum_i Y_m^l(\theta_i, \phi_i) = 0 , \quad m = -l, \cdots, l . \tag{39}$$

It remains to identify those values of l which contain the trivial representation. This is easily answered from an analysis of the characters of the group. The number of trivial representations n_A contained in the $l-$th representation of $SO(3)$ is given by

$$
\begin{aligned}
n_A(l) \quad = \quad & \frac{1}{60} \left\{ 2l + 1 + 12 \frac{\sin\left\{ (l+\frac{1}{2})\frac{2\pi}{5} \right\}}{\sin(\frac{\pi}{5})} + 12 \frac{\sin\left\{ (l+\frac{1}{2})\frac{4\pi}{5} \right\}}{\sin(\frac{2\pi}{5})} + \right. \\
& \left. 20 \frac{\sin\left\{ (l+\frac{1}{2})\frac{2\pi}{3} \right\}}{\sin(\frac{\pi}{3})} + 15 \sin\left\{ (l+\frac{1}{2})\pi \right\} \right\} ,
\end{aligned}
\tag{40}
$$

which is nonzero for $l = 6, 10, 12, 16$ and all even-l, $l > 16$ [31]. Note that Eq. (39) is satisfied for all l-odd modes, as follows from applying the inversion operator I, the generator of the C_i subgroup of $\mathcal{Y}_h$.

The icosahedral solution screens out the Gaussian curvature very effectively. Eq. (31) is partially satisfied, particularly for low l. The icosahedral lattice allows for non-zero contributions for only three ($l = 6, 10, 12$) of the first fifteen putative contributions in Eq. (30). A numerical evaluation gives the energy of an icosahedron $E^{\mathcal{I}}$ as

$$E^{\mathcal{I}} = 0.604 \left(\frac{\pi K_0}{36} R^2 \right) + 12\, E_{core} , \tag{41}$$

where E_{core} is the core energy of a single disclination. Its precise value is non-universal and depends on short distance details of the microscopic pair potential. The coefficient of $\pi K_0 R^2/36$ is universal, independent of short-distance properties. Let us study it in more detail. In Table 1 we show the relative contribution from each l-mode. It is apparent that the first allowed non-zero contribution $l = 6$ accounts for almost 80% of the total energy of the icosahedron. Note also the relatively rapid convergence of the expansion; truncating up to the $l = 100$ mode gives a result which differs by less than 0.2% from the actual result, Eq. (41). It is remarkable how much the energy would be reduced by canceling out the $l = 6$ mode without further enhancing higher l-modes.

l	$E_l^{\mathcal{I}}$	$E_t^{\mathcal{I}}$	l	$E_l^{\mathcal{I}}$	$E_t^{\mathcal{I}}$
6	0.4669	0.4669	30	0.0017	0.5925
10	0.0329	0.4999	40	0.0012	0.5975
12	0.0507	0.5506	50	0.0004	0.5997
16	0.0129	0.5635	80	0.0001	0.6025
18	0.0125	0.5760	100	3×10^{-5}	0.6031
20	0.0004	0.5764	∞	0	0.6043

Table 1: The first column is the particular mode considered. $E_l^{\mathcal{I}}$ is the contribution of the l-mode to the total energy and $E_t^{\mathcal{I}}$ the running sum after adding all modes less than or equal to l. For convenience we set $E_{core} = 0$ and $\pi K_0 R^2/36 = 1$ in this table.

5 Small core energies: The proliferation of defects

If the defect core energies are small then the elastic energy may be reduced by creating additional defects. The topological constraint Eq. (24) requires that additional defects appear in pairs of opposite charge. The challenge now is to understand and study the different possible distributions of these charges and the reduction in energy that those bring about when compared with the pure icosahedral case. The general form of the energy is, similarly to Eq. (41),

$$E = C \frac{\pi K_0 a^2}{36} \left(\frac{R}{a} \right)^2 + N E_{core} , \qquad (42)$$

where we introduce the C-coefficient as a convenient parametrization of the elastic part of the energy. In the limit $R/a \to \infty$, where a is the particle spacing, we expect grain boundaries containing $N \sim R/a$ dislocations emerging from each disclination. Hence the elastic term will *always* dominate over the core energy term in this limit. The critical sphere radius $R = R_c$ above which long range elastic energies dominate is given by $R_c \sim \text{const.}(36E_{core}/\pi K_0 a^2)a$.

If the total number of defects is large, an unconstrained minimization of Eq. (29) becomes an involved numerical problem. Instead of pursuing this further, we develop different approximations that allow us to tackle the case of a large number of defects while still capturing the most important features of the problem.

With results for a particular defect ansatz expressed as in Eq. (42), we need to determine the minimum distance of closest approach of neighboring plus-minus defect pairs. Upon identifying this distance with a, we can obtain the total number of particles M embodied in the defect configuration via the identification

$$M \approx \frac{8\pi}{\sqrt{3}a^2} R^2 \ . \tag{43}$$

5.1 The icosahedral approximation

Let us add new sets of twelve defects, each set lying on the vertices of an icosahedron. That is, we consider Eq. (29), not as a function of individual defects, but as a function of icosahedra of defects. From the mathematical arguments in the previous section, we can guarantee that the l-modes which vanish in the expansion Eq. (32) for the pure icosahedral case, will continue to do so within this approach. Since most of the low l-modes, which dominate the energy, vanish for any icosahedron, we expect that the Euler angles of the sets of icosahedra may be arranged to cancel the remaining non-vanishing low-l contributions. Our hope is that the energy bounds derived from this constrained problem provide a reasonable picture of the full unconstrained model.

If there are $n_+^{\mathcal{I}}$ icosahedra of fives, and $n_-^{\mathcal{I}}$ icosahedra of sevens, the topological constraint Eq. (24) becomes

$$n_+^{\mathcal{I}} - n_-^{\mathcal{I}} = 1 \ . \tag{44}$$

For a given configuration the energy is given by

$$E^{n\mathcal{I}} = C_{n\mathcal{I}} \frac{\pi K_0}{36} R^2 + 12(2n_+ - 1) E_{core} \tag{45}$$

where the C coefficient is a function of $3(n_+^{\mathcal{I}} + n_-^{\mathcal{I}} - 1) = 6n_+^{\mathcal{I}}$ variables. Let us first choose a distinguished icosahedron with explicit coordinates

$$(\theta, \phi) \equiv \left\{ (0, \text{any}), (\gamma, \frac{2\pi k}{5})_{0 \le k \le 4}, (\pi - \gamma, \frac{\pi}{5} + \frac{2\pi k}{5})_{0 \le k \le 4}, (\pi, \text{any}) \right\} \ , \tag{46}$$

where $\gamma = \cos^{-1}(1/\sqrt{5})$. Each of the remaining icosahedra may then be parametrized by the set of three Euler angles necessary to bring them to the position described by Eq. (46).
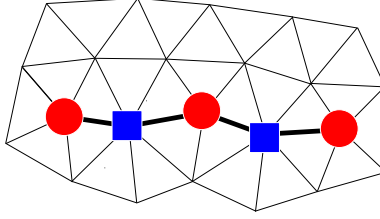
18

Figure 3: Particle configurations near a finite grain boundary. Circles represent five-coordinated sites and squares represent seven-coordinated sites.

The problem is to minimize over this set of Euler angles. We perform this minimization using a direction set algorithm [32]. From the results shown in Table 2, it is clear that the energy coefficient C is reduced by the addition of defects. It is therefore favorable to form defects for a sufficiently small core energy.

$n_+^{\mathcal{I}}$	Total	$C_{n_{\mathcal{I}_t}}$	a/R	M
1	12	0.60	γ	12
2	36	0.45	0.09	1791
3	60	0.38	0.06	4031
4	84	0.34	0.03	16124
5	108	0.30	0.02	36279
6	132	0.257	0.02	36279

Table 2: Table of results for the minimum energy coefficient, as defined in Eq. (45), obtained within the icosahedral approximation as a function of the number $n_+^{\mathcal{I}}$ of icosahedral clusters of positive charge. The The penultimate column gives the average geodesic distance between neighboring charges. The last column gives the corresponding total number of particles, as estimated from Eq.(43).

Another important issue is the precise arrangement of defects in the ground state. For $n_+ < 5$ we find the remarkable appearance of finite grain boundaries – finite strings of interlaced fives and sevens, as depicted schematically in Fig. 3. These grain boundaries are not always perfectly linear, although one does find alternating disclination chains clustered along geodesic line segments. Occasionally one finds dislocations, i.e. disclination pairs, displaced from this geodesic by a few lattice spacings. The ground state we

find, for the case $n_+ = 4$, is depicted in Fig. 4, and nicely illustrates the above features. Note that although the local structure of these grain boundaries mimics that expected for flat space, the curvature of the sphere allows these linear structures to terminate, consistent with the discussion in the Introduction.

For the case $n_+ = 5$ we still observe finite grain boundaries, but they show a tendency to spiral. This tendency becomes more pronounced for the case $n_+ = 6$, where the finite strings evolve into more complicated structures.

The picture emerging then within the icosahedral approximation is that small core energies favor a proliferation of defects. Below a critical number of defects of order 100, the ground state is well described by twelve finite grain boundaries, each one seeded by a defect in the original icosahedron. Above the critical number of defects the finite grain boundaries tend to branch and develop tentacles: the linear character of the pattern is lost.

5.2 String dominated regime

In this section we examine the relative orientation of the finite grain boundaries discussed in the previous section. One ansatz is provided by a solution having the form depicted in Fig. 5. There is an axis of three-fold rotational (C_3) symmetry at the center of the triangle formed by the geodesics connecting the three nearest-neighbor disclinations of the icosahedral array which forms the starting point of this variational ansatz. Finite grain boundaries are constructed by adding defects along the geodesic which joins the purely icosahedral sites with the center of C_3-symmetry. The midpoints of the grain boundaries form an icosahedron. The only free parameter in the model is the lattice spacing. This parameter may be fixed by minimizing the energy with respect to the lattice spacing,

$$\frac{dE(a)}{da} = 0 \ . \tag{47}$$

The interpretation of this extremal lattice spacing is discussed in Sec. 6.

The results from this minimization are shown in Table 3. When the total number of defects is less than a critical value (approximately 110) this C_3 solution has energies slightly lower than those found within the icosahedral approximation. This is remarkable if one recalls that this C_3-symmetric solution is obtained by minimizing with respect to only *one* parameter, the lattice spacing. The results obtained from the icosahedral approximation
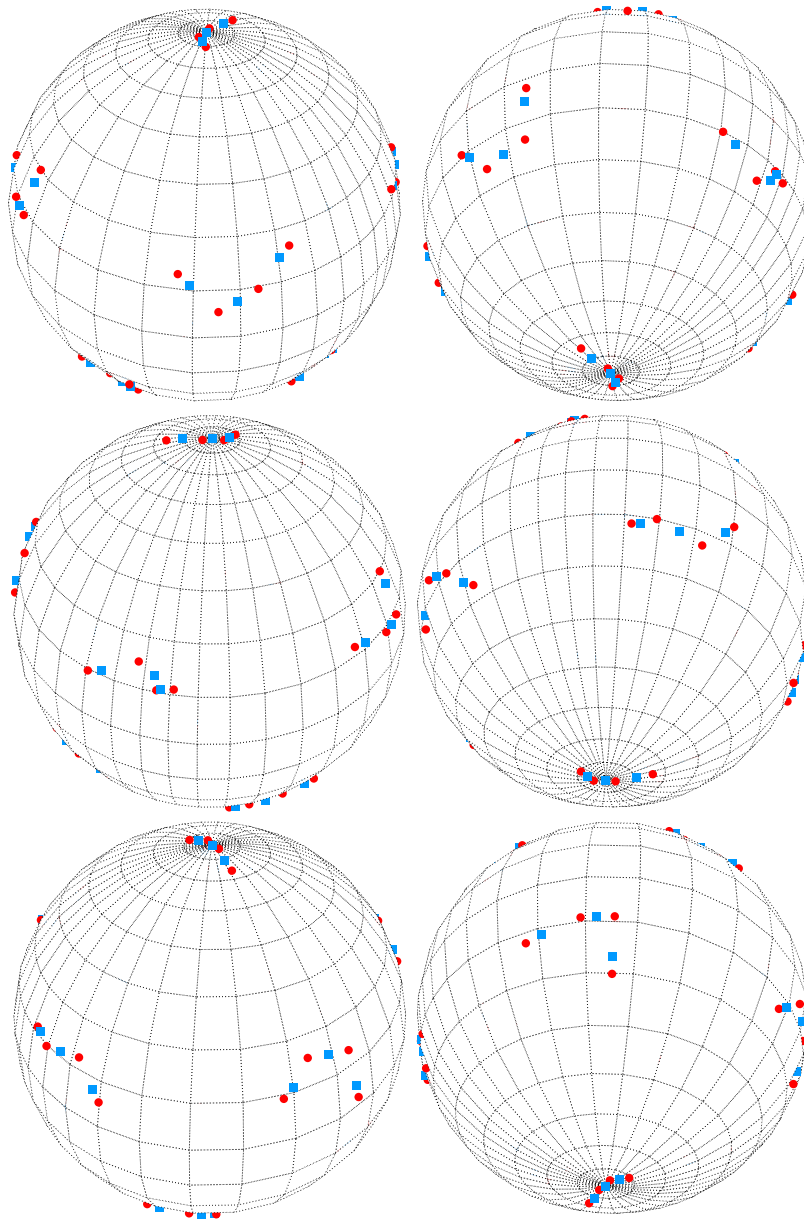
Figure 4: Six views of the ground state configuration for the icosahedral solution with seven sets of icosahedral defect clusters. The top figure in each column shows the north and south pole respectively. The subsequent views are obtained by successive rigid body 120° rotations of the entire sphere, using the right-hand rule, about an axis running from the north pole to the south pole.
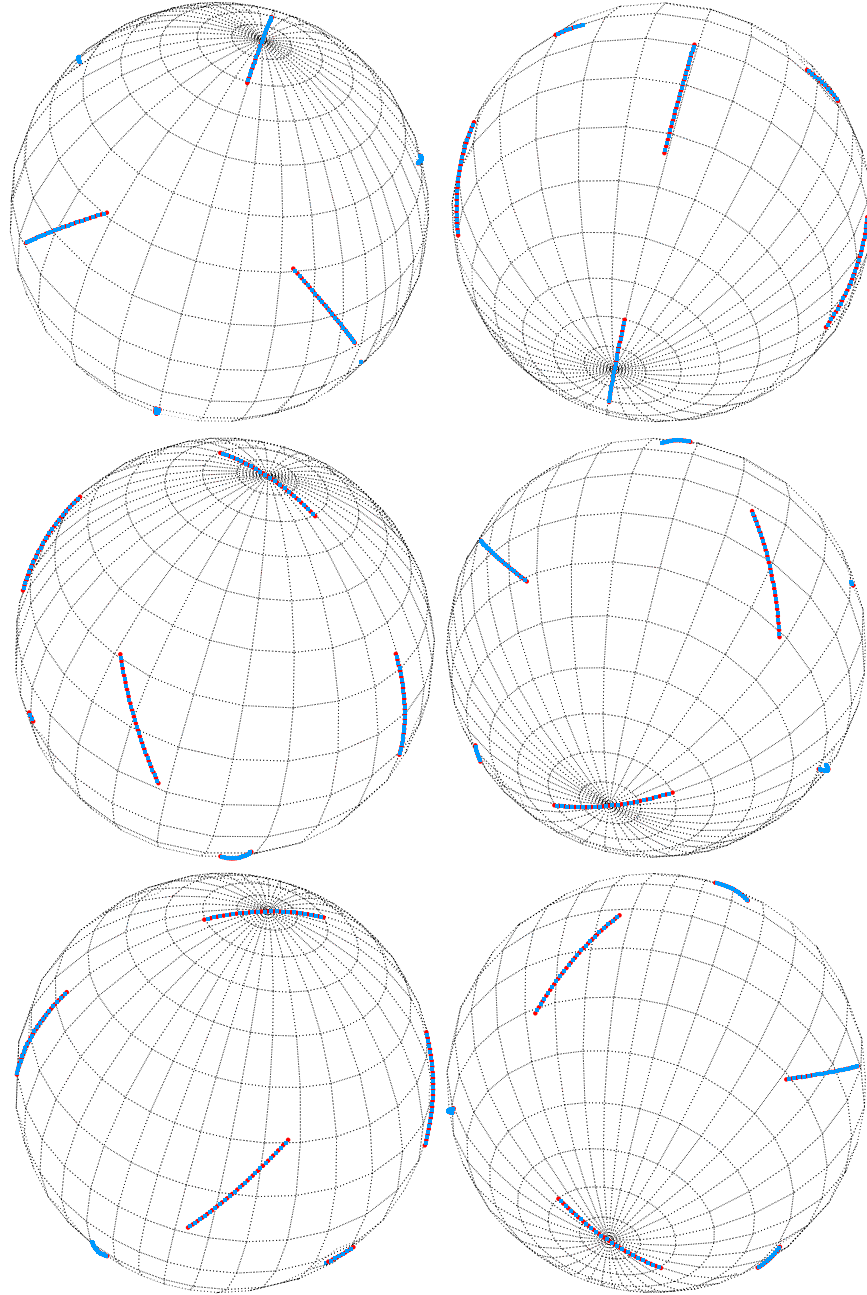
Figure 5: Six views of the ground state configuration for the C_3 solution with a large number of defects. The views are related as in Fig. 4.

Total	C	a
12	0.60	γ
36	0.44	0.121
60	0.37	0.085
84	0.34	0.062
108	0.32	0.051
132	0.31	0.042
252	0.28	0.024
492	0.26	0.012
972	0.255	0.006

Table 3: The minimum energy coefficient (see Eq. (45)) for the C_3 solution, as a function of the total number of defects. The last column gives the lattice spacing a as determined from Eq. (47).

itself are in rough agreement with this very simple ansatz, as apparent from Fig. 6. Table 3 also makes clear that there is little gain in energy when the total number of defects exceeds the critical value, even in the limit of a very large number of defects. This is consistent with the picture that purely linear finite grain boundaries are replaced by more complicated structures when the number of defects is large.

A more sophisticated treatment of *strings*, motivated by the discussion of dislocations in the Introduction, would build the grain boundaries from disclination dipoles with fixed size and then allow a variable spacing between these dislocations. We hope to pursue this approach in a future publication.

5.3 Large number of defects

We now have conclusive evidence that additional defects can lower the total energy of the system for small core energies. Defects will then proliferate and form highly complicated patterns. A detailed investigation of this regime is in progress, with complete results to be presented elsewhere. In this section we present one example of a branched structure that has lower energy than any of the linear structures considered so far. The structure we analyze consists of defects arranged in star patterns, or *pentagonal buttons* in the terminology of Toomre[12] (see Fig. 7). To study these structures we construct rings of five-disclinations forming a pentagon with its center at the position of the
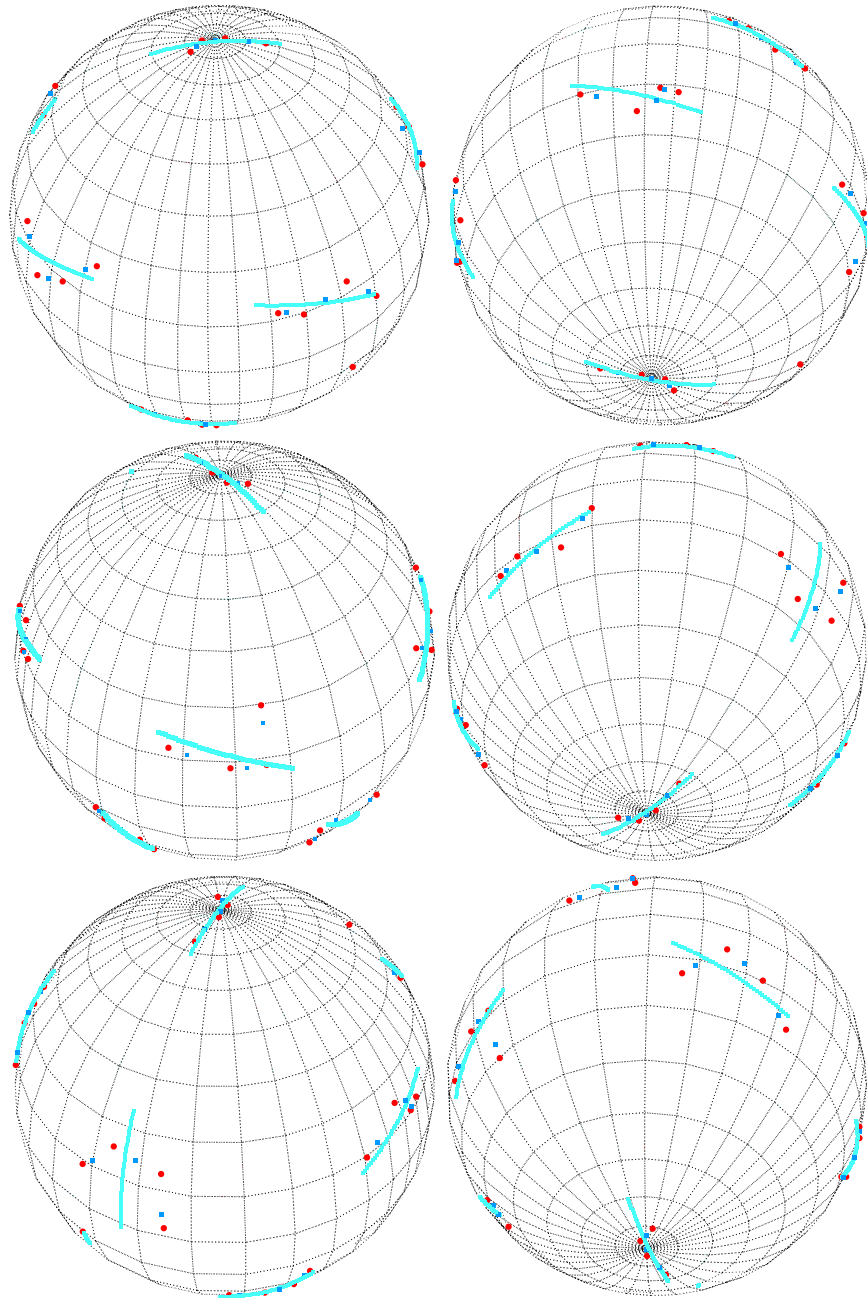
Figure 6: Six views of the ground state configuration for the superposition of the C_3 solution and the icosahedral solution Fig. 4. The views are related as in Fig. 4.

icosahedron, as shown in Fig. 7. As free parameters we leave the radius of each ring, and the angle each ring forms with a given geodesic joining the center of a star to that of its neighbor. The topological constraint Eq. (24) implies that there must be the same number of rings of fives as sevens.
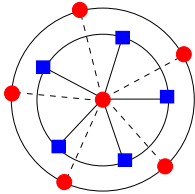

Figure 7: Example of a simple star defect with two rings, one of fives (circles) and one of sevens (squares).

From Table 4 we see the energy for 132 defects is marginally lower than the corresponding value for the icosahedral approximation. For more defects the star clusters have significantly lower energy than the C_3 solution. It is remarkable that all the disclinations in this ground state solution, other than the twelve seed disclinations, bind to form *radial* dislocations as illustrated in Fig. 8). Furthermore, the relative orientation of the different rings conform to a rhombic tiling of the sphere consisting of 30 completely regular diamonds (the *rhombic tricontahedron*), as shown in the bottom left picture of Fig. 8. Note that by minimizing the defect elastic energy we obtain a *dynamically generated* particle spacing, for a fixed sphere radius, which optimizes the given structure. Further investigation of these pentagonal buttons, as well as other more involved structures, will be presented in the future.

Total	C	a/R
132	0.255	0.04
252	0.170	0.025

Table 4: Table of results for the minimum energy coefficient, as defined in Eq. (45) obtained within star defects as a function of the total number of defects. The last column gives the value of the particle spacing a.

It is natural, at this point, to ponder the nature of the ground state in the limit of an infinite number of defects with vanishing core energy or, equivalently, in the limit $R/a \to \infty$. We have, in fact, already addressed this question in subsect. 3.2, where we proved that the only zero energy solution
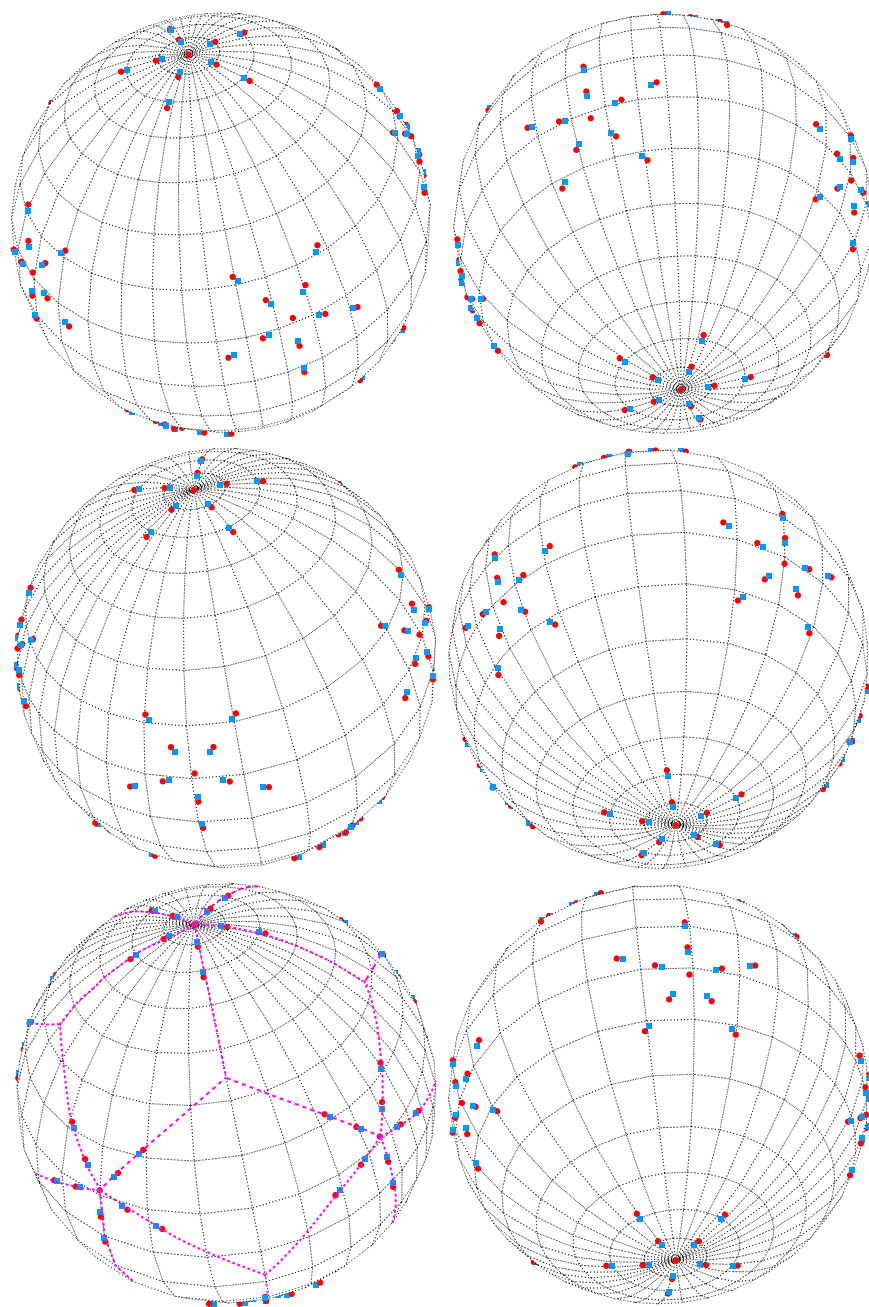
Figure 8: Six views of the ground state configuration for four rings of *pentagonal buttons*. The views are related as in Fig. 4. The bottom left view shows the associated rhombic tiling (the rhombic tricontahedron) of the sphere.

26

is an arrangement of defects $\{q_i, (\theta_i, \phi_i)\}_{i=1,\cdots}$ satisfying Eq. (31). In this case the defect density would be fully rotational invariant and screen out the Gaussian curvature completely. Currently we find solutions that seem to be converging to this limiting case, but it is open as to how accurately one can achieve the desired limit $C = 0$.

6 Instabilities of Icosahedral Lattices

Our discussion so far has focused entirely on analyzing the distribution of topological defects on the sphere. We turn our attention now to the implications for the underlying lattice structure. We thus take into account the regular six-fold coordinated nodes as well as the defects and examine the resultant lattices.
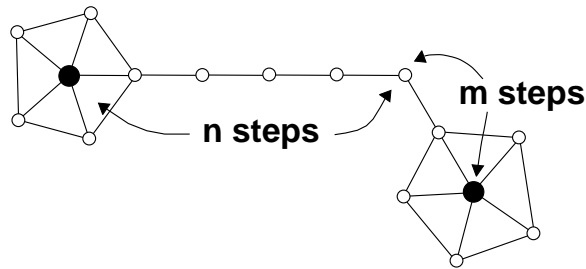

Figure 9: The construction of a type (n,m) icosadeltahedral lattice. The filled circles indicate two nearest-neighbor five-fold disclinations.

In the limit of large core energies our model predicts twelve disclinations forming an icosahedron. Lattices whose only defects are twelve positive disclinations sitting at the vertices of an icosahedron may be constructed easily, since they are characterized by the path between two nearest-neighbor disclinations. For a type (n, m) lattice this path consists of n straight steps from a given disclination, a 120° turn, and then m more straight steps to the nearest-neighbor disclination (see Fig. 9). The total number of particles M within this (n, m) (icosadeltahedral) lattice is

$$M = 10(m^2 + n^2 + mn) + 2 . \tag{48}$$

Within our model, the energy for these configurations has been computed in Eq. (41). Since the core energy is sensitive to the short-distances properties

of the model, different icosadeltahedral lattices will have different energies, even for an arbitrarily large number of particles.

Since most of the triangles in an icosadeltahedral lattice cannot be equilateral there is no uniquely defined lattice spacing. An average lattice spacing a can, however, be estimated. On the sphere, the distance between two nearest-neighbor disclinations is given by $R\gamma$ ($\gamma = \cos^{-1}(1/\sqrt{5})$). For the $(n, 0)$-case we have the relation $R\gamma = n \times a$, and therefore

$$a = \frac{R\gamma}{n} \ . \tag{49}$$

Any other sensible way of estimating the lattice spacing, such as the size of a disclination dipole, should give a value of the same order. In the following we restrict ourselves to $(n, 0)$ lattices for simplicity, but it is easy to generalize the formulas to arbitrary (n, m) icosadeltahedral lattices.
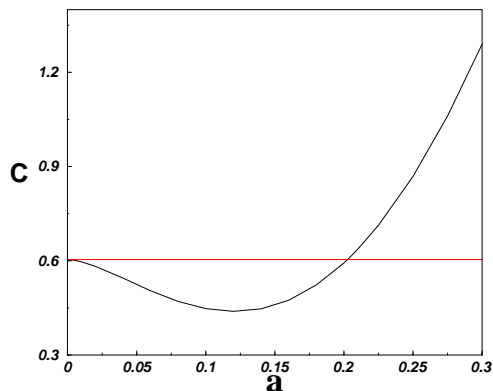

Figure 10: The C coefficient as a function of the lattice spacing for the C_3-solution corresponding to a 3 length finite grain boundary. The straight line corresponds to the C-coefficient for a pure icosahedron.

From previous sections we know that there will be a range of core energies for which the icosahedral lattices will be unstable to the formation of defects. To visualize this more clearly, let us take the C_3-solution of section 5.2 for the case of finite grain boundaries having just three defects (a 5-7-5 configuration), and plot the C-coefficient as a function of the lattice spacing. The result is shown in Fig. 10. For sufficiently large lattice spacings the C coefficient exceeds that of a single icosahedral lattice. As the lattice spacing

28

is reduced, there is a critical particle spacing a_*, such that the C coefficient of the C_3 solution becomes smaller than that of the pure icosahedral lattice. Restricting ourselves to the $(n, 0)$ icosadeltahedral configurations, we find from Fig. 10, Eq. (49) and Eq. (48)

$$a_*/R \sim 0.2 \rightarrow n(a_*) = 5.5 \rightarrow M(a_*) = 305 , \tag{50}$$

where we explicitly display the dependence on a_*. This result implies that the pure $(n, 0)$ icosadeltahedral lattice is unstable to the formation of defects for sufficiently small core energies and more than 316 particles. Alternatively, Eq. (43) gives $M = 363$, consistent with the estimate above. Let us point out that the minimum of the energy occurs at lattice spacing $a_c = 0.121$ (number of particles $M_c = 1256$). For lattice spacings below a_c the disclinations will prefer to remain separated by a distance a_c. This is accomplished by stringing six-fold coordinated particles between defects. Since lower energy configurations may be formed by allowing interpolating dislocations instead, we regard M_c as the maximum number of particles for which this particular structure is stable. The particle numbers quoted in the tables of Sec. 5 should be interpreted as the corresponding M_c.

This shows that the minimum of the energy is attained for lattice spacings smaller than those necessary for stability. Finally, in the limit of vanishing lattice spacing, the C_3-solution becomes equivalent to a pure icosahedron, and both C-coefficients merge.

7   The Thomson problem

The Thomson problem can be stated as finding the ground state of an arbitrary number of positive charges interacting through the usual 3d Coulomb potential, but with the further constraint that these charges must lie on a sphere. Since this problem falls within the universality class of our model it serves as a good testing ground.

The Thomson problem has proven to be extremely difficult to analyze numerically, basically because of the large number of metastable states. Early analyses [10] showed that the ground state of the system for small numbers of charges was an icosadeltahedral lattice. Since a small number of charges corresponds to a large particle spacing this follows from our model as well. Some rules were also conjectured to decide on the true ground state when several icosadeltahedral lattices were possible for a given number of charges.

These rules could be examined within our model provided we are able to isolate the dependence of the core energy on the lattice type.

Subsequent numerical work [11] provided convincing evidence that the ground state, for a sufficiently large number of charges, does not have icosahedral symmetry. The critical number of charges for which additional defects arise seems to be around 400 [12], which is in agreement with our results. It is also found that these additional defects first arrange themselves into finite grain boundaries [12], as seen in our model. For more charges the ground state in the Thomson problem becomes very complex and the true ground state is not known. New configurations (one of the simplest being *pentagonal buttons*) appear to be energetically favorable in the early stages of this limit. This observation [12] is in agreement with our model as well.

In the work of [12] (see also [13]) it is also observed that the ground state energy for a large number of charges seems to converge to the energy that one would obtain in the unrealizable situation that all the charges are located on equilateral triangles. This limit corresponds to the defect density completely screening out the Gaussian curvature. The defect density therefore satisfies Eq. (31), which we proved is the absolute minimum of our model in the limit of vanishing core energy.

We think that the comparison of our model with the Thomson problem is very promising, but requires more detailed investigation to be addressed in the future.

8 Discussion and Conclusions

In this paper our first task was to propose and study an effective free energy for disclination defects in particle arrays constrained to move on the surface of a two-dimensional sphere. The finite-temperature problem does not seem to be analytically solvable but we propose a discretized Laplacian Sine-Gordon model amenable to direct numerical methods. The structure of the ground state may, however, be studied analytically. This structure depends on the ratio of disclination core energies to the Young's modulus. On the sphere topology demands there be a total excess disclinicity charge of twelve. This excess charge can seed new ground state structures, compared to flat space. For large core energies (or $R/a \leq 36E_{core}/(\pi K_0 a^2)$) the disclinations arrange themselves to form an icosahedron. For intermediate core energies (i.e. $R/a \geq 36E_{core}/(\pi K_0 a^2)$) grain boundaries develop which

30

terminate freely within the medium. The regime of still lower core energies, corresponding to $R/a \to \infty$, was found to be surprisingly complex – new defect arrangements make their appearance.

Currently we are actively investigating the regime of small or vanishing defect core energy, including a detailed comparison of the predictions of our model with numerical results from the Thomson problem. A rigorous determination of the ground state for the Thomson problem is presently computationally prohibitive when the particle numbers exceed $\mathcal{O}(500)$. Our methods enable us to reach particle numbers of $\mathcal{O}(10,000)$ or more with the same computational effort.

Finally we believe that the rich symmetry structure underlying Eq. (31) may provide a direct analytic determination of the exact ground state in the limit of a large number of particles and further work in this direction is certainly warranted.

Acknowledgements

A The infinite radius limit

In this Appendix we discuss in more detail the large R limit of the energy function Eq. (29). It is readily seen from dimensional analysis and linearity that the χ function of Eq. (28) scales like R^2.

Now consider a single isolated disclination q_1 located at point P_1 on the sphere, together with a single dislocation, with Burgers vector $\mathbf{b}_2$, located at point P_2. From Eq. (29) the total energy is

$$E = \frac{\pi K_0}{36} \left(q_1^2 R^2 + |\mathbf{b}_2| q_1 f(P_1, P_2) R + |\mathbf{b}_2|^2 \log \left(\frac{R}{2a} \right) \right) , \qquad (51)$$

where $f(P_1, P_2)$ is a function whose explicit form does not matter for the present analysis. The quadratic R dependence comes from the isolated disclination, the linear R dependence comes from the dislocation-disclination interaction and the logarithmic term comes from the dislocation energy. In the infinite-radius limit of the sphere we see, therefore, that the various defect energies scale identically to those in a flat space system of size R [20, 26]. The nature of the ground state, however, is dramatically changed.

B The biharmonic operator on the sphere

The evaluation of the inverse biharmonic operator on the sphere is rather tedious. We outline the steps for a sphere of unit radius. The simplest approach is to first compute the inverse harmonic operator. The sum over m is performed as in Eq. (26). The result involves only Legendre polynomials and is

$$\Gamma(x) \equiv \frac{1}{4\pi\Delta} = \sum_{l=0}^{\infty} (\frac{1}{l+1} + \frac{1}{l}) P_l(x). \qquad (52)$$

The sums over l may be performed using the identities

$$\sum_{l=0}^{\infty} \frac{1}{l+1} P_l(x) = \int_0^1 du \frac{1}{(1 - 2ux + u^2)^{1/2}} \qquad (53)$$

and

$$\sum_{l=1}^{\infty} \frac{1}{l} P_l(x) = \lim_{\epsilon \to 0} (\int_\epsilon^t du \frac{1}{u(1 - 2ux + u^2)^{1/2}} - \int_\epsilon^1 \frac{du}{u}) . \qquad (54)$$

32

The resultant integrals are readily evaluated, yielding

$$\Gamma(x) = -\log(\frac{1-x}{2}) - 1 \; . \tag{55}$$

The inverse biharmonic operator now follows from the result $\Delta\chi(x) = \Gamma(x)$.

C The evaluation of χ

Performing a trivial integration by parts in Eq. (28), we get

$$\chi(\beta) = 1 + t(\log(t) - 1) + \int_0^t dz \frac{z \log z}{1 - z} \; , \tag{56}$$

with $t = \frac{1 - \cos\beta}{2}$. The last integral may be expressed via a change of variables as

$$\int_0^x dz \frac{z \log z}{1 - z} = -\int_u^\infty dx \frac{x e^{-x}}{e^x - 1} \; , \tag{57}$$

with $u = ln(1/t)$. Finally one can expand for small u and large u as

$$\int_u^\infty \frac{x e^{-x}}{e^x - 1} = \begin{cases} \frac{\pi^2}{6} - (u - \frac{u^2}{4} + \sum_{k=1} B_k \frac{u^{2k+1}}{(2k+1)!}) - e^u(u+1) \\ \sum_{n=1}(u + \frac{1}{n+1}) \frac{e^{-(n+1)u}}{n+1} \end{cases} \; , \tag{58}$$

where B_k are the Bernoulli numbers. These expansions are very useful as they allow a numerical evaluation of χ with arbitrary precision with negligible computational time. In fact we save, on average, a factor of 2000 in time compared to a direct evaluation of the integral using Romberg integration.

References

[1] D. R. Nelson and B. I. Halperin, Phys. Rev. B **19**, 2457 (1979); J. Kosterlitz and D. Thouless, J. Phys. C **6**, 1181 (1973); A. Young, Phys. Rev. B **19**, 1855 (1979).

[2] For reviews, see D. R. Nelson, in *Phase Transitions and Critical Phenomena*, Vol. 7, edited by C. Domb and J. Lebowitz (Academic, New York, 1983) and *Bond-Orientational Order in Condensed Matter Systems*, edited by K. J. Strandburg (Springer, New York, 1992).

[3] D. R. Nelson, in *Topological Disorder in Condensed Matter*, edited by F. Yonezawa and T. Nonomiya (Springer, Berlin, 1983).

[4] D. R. Nelson, Phys. Rev. B **28**, 5515 (1983).

[5] S. Sachdev and D. R. Nelson, J. Phys. C: Solid State Phys. **17**, 5473 (1984).

[6] M. J. W. Dodgson, J. Phys. A**29**, 2499 (1996) (http://xxx.lanl.gov/abs/cond-mat/9512124).

[7] F. C. MacKintosh and T. C. Lubensky, Phys. Rev. Lett. **67**, 1169 (1991); J. Park, T. C. Lubensky, and F. C. MacKintosh, Europhys. Lett. **20**, 279 (1992)(http://xxx.lanl.gov/abs/cond-mat/9606105).

[8] M. J. W. Dodgson and M. A. Moore, Phys. Rev. B**55**, 3816 (1997) (http://xxx.lanl.gov/abs/cond-mat/9512123).

[9] J. J. Thomson, Philos. Mag. **7**, 237 (1904).

[10] L. L. Whyte, Am. Math. Monthly **59**, 606 (1952); L. T. Wille, Nature **324**, 46 (1986); T. Erber and G. M. Hockney, J. Phys. A**24**, L1369 (1991) and Phys. Rev. Lett. **74**, 1482 (1995); L. Glasser and A. G. Every, J. Phys. A**25**, 2473 (1992); J. R. Edmundson, Acta Crystallogr. A**49**, 648 (1993); E. L. Altschuler, T. J. Williams, E. R. Ratner, F. Dowla and F. Wooten, Phys. Rev. Lett. **72**, 2671 (1994).

[11] A. Pérez-Garrido, M.J.W. Dodgson and M. A. Moore, Phys. Rev. B **56**, 3640 (1997) (http://xxx.lanl.gov/abs/cond-mat/9701090).

[12] Alar Toomre, private communication and to be published.

[13] A. Pérez-Garrido and M. A. Moore, *Symmetric patterns of dislocations in Thomson's problem* (http://xxx.lanl.gov/abs/cond-mat/9905217).

[14] A. A. Koulakov and B. I Shklovskii, Phys. Rev. B**57**, 2352 (1998) (http://xxx.lanl.gov/abs/cond-mat/9707204).

[15] See, e.g. *Statistical Mechanics of Membranes and Surfaces*, edited by D. R. Nelson, T. Piran, and S. Weinberg, Jerusalem Winter School for Theoretical Physics Vol. 5 (World Scientific, Singapore, 1989).

[16] C. Carraro and D. R. Nelson, Phys. Rev. E **48**, 3082 (1993) and references therein (http://xxx.lanl.gov/abs/cond-mat/9307008).

[17] S. B. Dierker, R. Pindak and R. B. Meyer, Phys. Rev. Lett. **56**, 1819 (1986).

[18] F. L. Somer, G. S. Canright and T. Kaplan, Phys. Rev. E**58**, 5748 (1998) (http://xxx.lanl.gov/abs/cond-mat/9809179).

[19] We note that grain boundaries have also been proposed as an alternative mechanism for two dimensional melting when the core energy is small (see S. T. Chui, Phys, Rev. B **28**, 178 (1983)). Low angle grain boundaries, however, only become thermodynamically favorable (in the sense that their free energy changes sign) at precisely the unbinding temperature of dislocation pairs invoked in the conventional dislocation unbinding theory. See D. S. Fisher, B. I. Halperin and R. Morf, Phys. Rev. B**20**, 4692 (1979).

[20] H. S. Seung and D. R. Nelson, Phys. Rev. A**38**, 1005 (1988).

[21] See, e.g., R. Bruinsma, B. I. Halperin, and A. Zippelius, Phys. Rev. B**25**, 579 (1982), and references therein.

[22] We assume for simplicity a finite concentration of vacancies and interstitials so that the pair can separate via climb motion. If climb is frozen out kinetically, the dislocations can still separate via glide motion. The binding potential has an angular dependence in this case. See Ref.[21].

[23] U. Albrecht and P. Leiderer, J. Low Temp. Physics 86, 131 (1992); P. Leiderer, Zeitschrift fur Physik B**98**, 303 (1993).

[24] M. J. Bowick and A. Travesset, *The Geometric Structure of 2D Bond-Orientational Order*, Syracuse University preprint SU-4240-709.

[25] D. R. Nelson and L. Peliti, J. de Physique **48**, 1085 (1987).

[26] D. R. Nelson, Phys. Rev. B **26**, 269 (1982).

[27] For Monte Carlo simulations in flat space, see K. J. Strandburg, Phys. Rev. B **35**, 7161 (1986).

[28] A. Pérez-Garrido and M. A. Moore, Phys. Rev. B **58**, 9677 (1998) (http://lanl.gov/abs/cond-mat/9802167).

[29] J. Park and T. C. Lubensky, Phys. Rev. E **53**, 2648 (1996) (http://xxx.lanl.gov/abs/cond-mat/9512108).

[30] Our results differ from those in Appendix A of Ref.[6].

[31] P. Steinhardt, D. R. Nelson and M. Ronchetti, Phys. Rev. B **28**, 784 (1983).

[32] *Numerical Recipes in C*, W. H. Press, B. P. Flannery, S. A. Teukolsky and W. T. Vetterling (Cambridge University Press, Cambridge, 1988).

[33] M. Phillips, S. Levy and T. Munzer: Geomview: an interactive geometry viewer, Notices of the American Monthly Society **40** (1993) 985-988 (http://www.geom.umn.edu/).